Eur. Phys. J. D **21**, 57–61 (2002)
DOI: 10.1140/epjd/e2002-00184-1

THE EUROPEAN
PHYSICAL JOURNAL D

Measurements of L subshell and total L shell photoeffect cross-sections for some elements in $72 \leq Z \leq 92$

A. Karabulut[1], A. Gürol[1,a], G. Budak[1], and R. Polat[2]

[1] Atatürk University, Faculty of Art and Science, Department of Physics, 25240 Erzurum, Turkey
[2] Atatürk University, Erzincan Education Faculty, Erzincan, Turkey

Received 15 February 2002 / Received in final form 10 June 2002
Published online 24 September 2002 –

Abstract. We determined L subshell photoeffect cross-sections by using Lα, Lγ_1, and L$\gamma_{2,3,6,8}$ X-ray fluorescence cross-sections and atomic parameters and total L shell photoeffect cross-sections for Hf, Hg, Tl, Bi, Tl, and U at 59.54 keV. These values were compared with the theoretical values of Scofield and experimental values that exist in the literature.

PACS. 32.80.Cy Atomic scattering, cross-sections, and form factors; Compton scattering

1 Introduction

The photoeffect phenomenon has been studied since the photoeffect cross-section is an important parameter in X-ray Fluorescence (XRF) analysis. Values of cross-sections for the photoeffect of inner shell electrons are required for radiation physics, nuclear physics, energy transport and deposition calculations, dosimetry, and elemental analysis of materials using X-ray emission techniques. The numerical data of Scofield [1] on the total and subshell photoeffect cross-sections are considered to be most accurate theoretical data [2]. These data include elements of $Z = 1$ to 101 in the energy region 1 to 1 500 keV. On the other hand, K shell, L shell and total L shell photoeffect cross-sections have been determined experimentally by many workers using photons and accelerated particles [2–20]. The accurate and reliable data on the L XRF cross-sections have an important bearing in the theory for developing more realistic models describing the fundamental processes following inner-shell ionisation, namely, radiative, Auger, and Coster Kronig [1]. A better approach to check parameters is to measure the XRF cross-sections for the X-rays originating from the individual L$_i$ ($i = 1, 2, 3$) subshell and total L shell.

In the present study, Lα, Lγ_1, L$\gamma_{2,3,6,8}$, L$\gamma_{4,4'}$, and Lγ_5 XRF cross-sections for elements in the atomic region $72 \leq Z \leq 92$ (namely, Hf, Hg, Tl, Bi, Th, and U) at 59.54 keV incident photon energy have been experimentally measured using an Energy Dispersive XRF (EDXRF) setup including ^{241}Am radioisotope source as exciter. Then, we calculated L subshell and total L shell photoeffect cross-sections by using Lα, Lγ_1, and L$\gamma_{2,3,6,8}$ XRF cross-sections and atomic parameters since there are insufficient works on L subshell and total L shell photoeffect cross-sections at 59.54 keV.

[a] e-mail: agurol@atauni.edu.tr

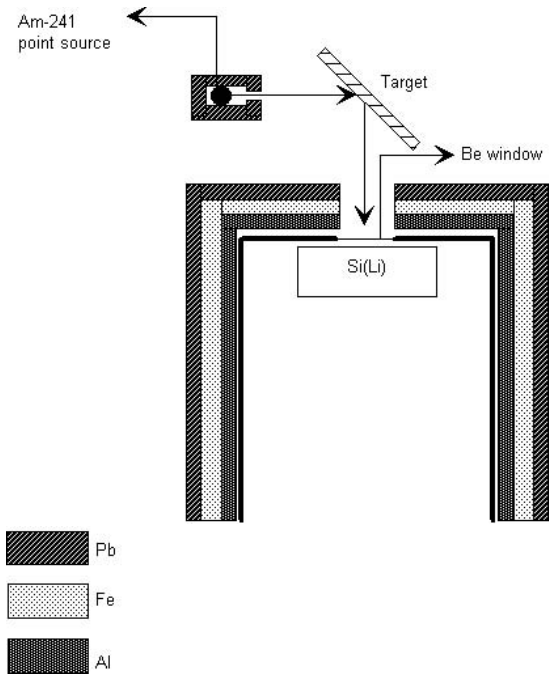

Fig. 1. Experimental setup.

2 Experimental technique

As shown in Figure 1, the experimental set-up consists of a point ^{241}Am radioisotope source with 100 mCi activity and gamma photon energy 59.54 keV, a Si(Li) solid-state detector of 12.5 mm^2 active area and a resolution of 160 eV at 5.9 keV Mn Kα line, and a sample. The detector coupled to a ND 66B 1024 multichannel analyser. The direct beams from the source mentioned above were incident on the sample. The samples were placed at a 45°

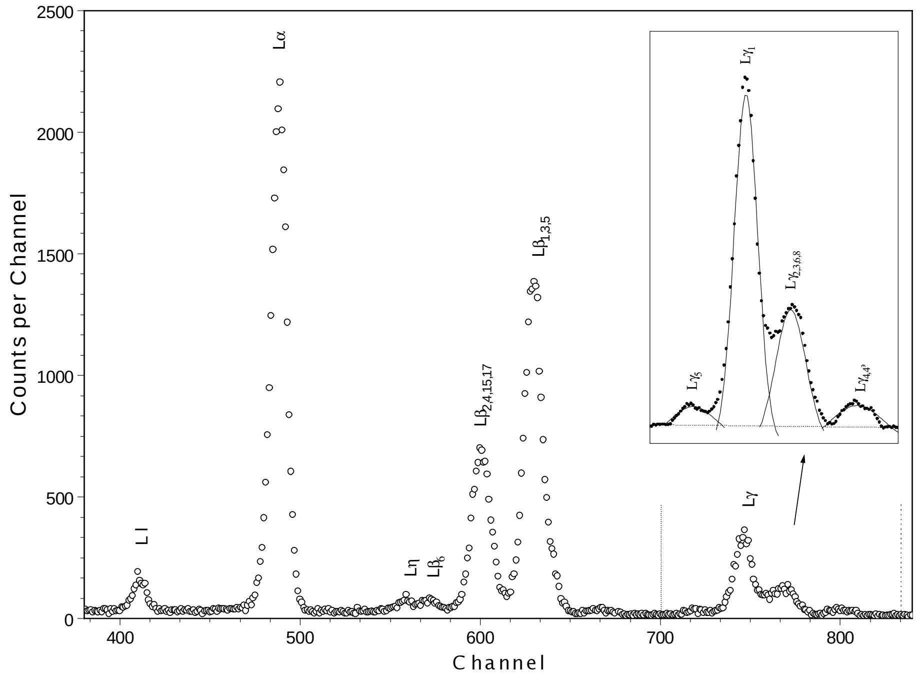

Fig. 2. A typical spectrum of U.

to the direct beam from the source and fluorescent X-rays emitted at 90° with respect to the direct beam from the source were detected by a Si(Li) solid-state detector. The samples used were spectroscopically high purity (∼99.9%) and in the form of powder evaporated on mylar backing. A typical L X-ray spectrum of U is shown in Figure 2. The counts under the peaks of various X-ray lines were estimated by both Gaussian and Gaussian with a tail assuming a polynomial background. To reduce the statistical error in the measurements, five spectra were recorded for each target and the live time was 10 h. Further, to minimize the systematic errors, if any, spectra for each target were taken on three different occasions. The thickness of the powders used in the experiment was about 25 μm.

3 Data analysis

The spectrum of L X-rays shown in Figure 2 contains four groups; *i.e.* Lℓ, Lα, Lβ, and Lγ groups of L X-rays. The Lγ group of X-rays consists of four components as shown in Figure 2's inset, that is, Lγ_1, L$\gamma_{2,3,6,8}$, L$\gamma_{4,4'}$, and Lγ_5. Lγ_1 and Lγ_5 are related to the L_{II} subshell, L$\gamma_{4,4'}$ are related to the L_I subshell, and L$\gamma_{2,3,6,8}$ is related to both L_I and L_{II} (L$\gamma_{2,3}$ is related to the L_I and L$\gamma_{6,8}$ is related to the L_{II}). The spectra were analysed by using Origin Software Program. As shown in the Figure 2's inset, a linear background is placed below the spectra of the L X-rays, from the first to the last channel. The mean of ten channels at each side of the overlapped peaks was used to calculate the background and to define the peak [21]. The composite Lγ peaks have been analysed into four Gaussians as shown in Figure 2's inset. In addition, the composite Lγ peaks have been fitted into four Gaussians and exponential tailings in their low-energy sides [22,23].

L-subshell photoeffect cross-sections were calculated by using the following equations [13]

$$\sigma_{\mathrm{L_I}} = \left[\sigma_{\mathrm{L}\gamma_{2,3,6,8}} - \sigma_{\mathrm{L}\gamma_1}\frac{\Gamma_{\mathrm{L}\gamma_{6,8}}}{\Gamma_{\mathrm{L}\gamma_1}}\right]\frac{\Gamma_1}{\Gamma_{\mathrm{L}\gamma_{2,3}}}\frac{1}{\omega_1} \quad (1)$$

$$\sigma_{\mathrm{L_{II}}} = \sigma_{\mathrm{L}\gamma_1}\frac{1}{\omega_2}\frac{\Gamma_2}{\Gamma_{\mathrm{L}\gamma_1}} - f_{12}\sigma_{\mathrm{L_I}} \quad (2)$$

$$\sigma_{\mathrm{L_{III}}} = \frac{\sigma_{\mathrm{L}\alpha}}{\omega_3}\frac{\Gamma_3}{\Gamma_{\mathrm{L}\alpha}} - (f_{13} + f_{12}f_{23})\sigma_{\mathrm{L_I}} - f_{23}\sigma_{\mathrm{L_{II}}} \quad (3)$$

$$\sigma_{\mathrm{L_T}} = \sigma_{\mathrm{L_I}} + \sigma_{\mathrm{L_{II}}} + \sigma_{\mathrm{L_{III}}} \quad (4)$$

where f_{ij} $(i \neq j = 1,2,3)$ are Coster-Kronig transition probabilities, ω_i $(i = 1,2,3)$ are L subshell fluorescence yields, Γ_i $(i = 1,2,3)$ are theoretical total radiative transition rates of L_i $(i = 1,2,3)$, $\Gamma_{\mathrm{L}\alpha}$, $\Gamma_{\mathrm{L}\gamma_1}$, $\Gamma_{\mathrm{L}\gamma_{2,3}}$, $\Gamma_{\mathrm{L}\gamma_{6,8}}$, and $\Gamma_{\mathrm{L}\gamma_{4,4'}}$ are theoretical total irradiative transition rates of the appropriate peaks, and $\sigma_{\mathrm{L}\alpha}$, $\sigma_{\mathrm{L}\gamma_1}$, and $\sigma_{\mathrm{L}\gamma_{2,3,6,8}}$ are the L X-ray fluorescence cross-sections determined experimentally.

$\sigma_{\mathrm{L}\gamma_1}$, $\sigma_{\mathrm{L}\gamma_{2,3,6,8}}$ and $\sigma_{\mathrm{L}\alpha}$ XRF cross-sections are experimentally determined using [24]

$$\sigma_{\mathrm{L}_i} = \frac{I_{\mathrm{L}_i}}{I_0 G \varepsilon_{\mathrm{L}_i}\beta t} \quad (5)$$

where I_{L_i} is the observed intensity (area under peak) corresponding to the L_i group of X-rays, $I_0(E)$ is the intensity of the incident radiation at the excitation energy, G is the geometric factor that influences the relative importance of absorption of the primary and secondary (analyte-line) X-rays [25], $\varepsilon_{\mathrm{L}_i}$ is the detection efficiency of the L_i group of X-rays and β is the self-absorption correction factor for the target material which accounts for the absorption in

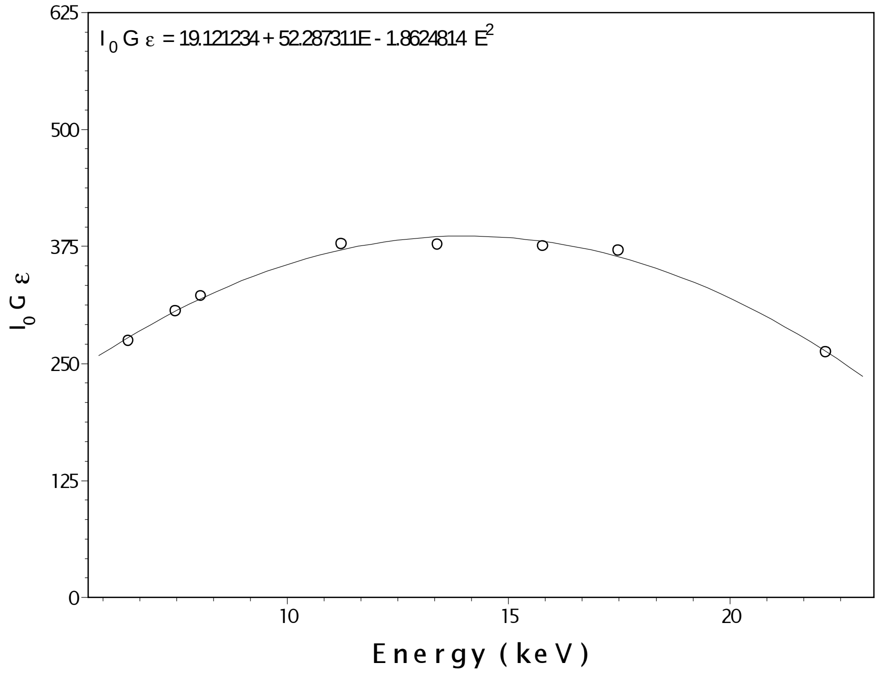

Fig. 3. Efficiency curve of Si(Li) detector.

the target of the incident photons and the emitted characteristic X-rays [24],

$$\beta = \frac{1 - \exp\left[-h_z(E_i)t\right]}{h_z(E_i)t} \tag{6}$$

$$h_z(E_i) = \left[\mu_{\mathrm{inc}} \sec\theta_1 + \mu_{\mathrm{emit}} \sec\theta_2\right] \tag{7}$$

where μ_{inc} and μ_{emit} are the mass absorption coefficients of the incident photons and the emitted characteristic X-rays in the target, respectively, taken from Hubbell and Seltzer [26]. θ_1 and θ_2 are the angles of the incident photons and the emitted characteristic X-rays with respect to the normal at the surface of the sample. These angles are equal to 45° in the present sample and t is the thickness of the sample. The value of the factor $I_0 G\varepsilon$ was determined by collecting the K X-ray spectra of thin samples of Fe, Ni, Cu, Rb, Mo, and Ag, and by using the relation [24]

$$I_0 G\varepsilon_{\mathrm{K}\alpha} = \frac{I_{\mathrm{K}\alpha}}{\sigma_{\mathrm{K}\alpha}\beta_{\mathrm{K}\alpha}t} \tag{8}$$

where the terms $I_{\mathrm{K}\alpha}$, $\beta_{\mathrm{K}\alpha}$, and $\varepsilon_{\mathrm{K}\alpha}$ have the same meaning as in equation (5), except that they correspond to K X-rays instead of the ith group of L X-rays. Theoretical values of ($\sigma_{\mathrm{K}\alpha}$) XRF cross-sections were obtained using the relation

$$\sigma_{\mathrm{K}\alpha} = \sigma_{\mathrm{K}}(E)\omega_{\mathrm{K}}F_{\mathrm{K}\alpha} \tag{9}$$

where $\sigma_{\mathrm{K}}(E)$ is the theoretical K shell photoeffect cross-sections taken [27] for the given element at the excitation energy E, ω_{K} is the K shell fluorescence yields [28], and $F_{\mathrm{K}\alpha}$ is the fractional X-ray emission rate for Kα X-rays, defined as

$$F_{\mathrm{K}\alpha} = \left[1 + \frac{I_{\mathrm{K}\beta}}{I_{\mathrm{K}\alpha}}\right]^{-1} \tag{10}$$

where $I_{\mathrm{K}\beta}/I_{\mathrm{K}\alpha}$ is the theoretical Kβ to Kα X-ray intensity ratio. In the Figure 3, it's shown the curve and equation of $I_0 G\varepsilon$ *versus* energy in keV.

L XRF cross-sections are theoretically calculated by using following equations [24]

$$\sigma_{\mathrm{L}\ell} = \left(\sigma_{\mathrm{L_I}}f_{13} + \sigma_{\mathrm{L_I}}f_{12}f_{23} + \sigma_{\mathrm{L_{II}}}f_{23} + \sigma_{\mathrm{L_{III}}}\right)\omega_3F_{3\ell} \tag{11}$$

$$\sigma_{\mathrm{L}\alpha} = \left(\sigma_{\mathrm{L_I}}f_{13} + \sigma_{\mathrm{L_I}}f_{12}f_{23} + \sigma_{\mathrm{L_{II}}}f_{23} + \sigma_{\mathrm{L_{III}}}\right)\omega_3F_{3\alpha} \tag{12}$$

$$\sigma_{\mathrm{L}\beta} = \sigma_{\mathrm{L_I}}\omega_1F_{1\beta} + \left(\sigma_{\mathrm{L_I}}f_{12} + \sigma_{\mathrm{L_{II}}}\right)\omega_2F_{2\beta} + \left(\sigma_{\mathrm{L_I}}f_{13} + \sigma_{\mathrm{L_I}}f_{12}f_{23} + \sigma_{\mathrm{L_{II}}}f_{23} + \sigma_{\mathrm{L_{III}}}\right)\omega_3F_{3\beta} \tag{13}$$

$$\sigma_{\mathrm{L}\gamma} = \sigma_{\mathrm{L_I}}\omega_1F_{1\gamma} + (\sigma_{\mathrm{L_I}}f_{12} + \sigma_{\mathrm{L_{II}}})\omega_2F_{2\gamma} \tag{14}$$

where the σ_{L_i} $(i = 1, 2, 3)$ are the L subshell photoeffect cross-sections, ω_1, ω_2, and ω_3 are the L subshell fluorescence yields, f_{12}, f_{13}, and f_{23} are the Coster-Kronig transition probabilities [28], and F_{ny} $(F_{3\ell}, F_{3\alpha}, F_{3\beta}$, etc.) are the fractions of the radiation width of the subshell contained in the yth spectral line, *i.e.*

$$F_{ny} = \Gamma_{ny}/\Gamma_n, \quad (F_{3\alpha} = \Gamma_{3\alpha}/\Gamma_3). \tag{15}$$

Here, Γ_3 is the theoretical total radiative transition rate of the $\mathrm{L_{III}}$ subshell and $F_{3\alpha}$ is the sum of the radiative transition rates that contributes to the Lα lines associated with hole filling in the $\mathrm{L_{III}}$ subshell, that is,

$$F_{3\alpha} = \left[\Gamma_3\left(\mathrm{M_{IV}} - \mathrm{L_{III}}\right) + \Gamma_3\left(\mathrm{M_V} - \mathrm{L_{III}}\right)\right]/\Gamma_3 \tag{16}$$

is the radiative transition rate from the $\mathrm{M_{IV}}$ and $\mathrm{M_V}$ subshell to the $\mathrm{L_{III}}$ subshell. Scofield, who applied relativistic Hartree-Slater theory with a central potential and included retardation, has calculated the radiative transition rates for many elements [30] and we used these values to obtained the F_{ny}.

Table 1. The values of σ_{L_I}, $\sigma_{L_{II}}$, $\sigma_{L_{III}}$, and σ_{L_T} photoeffect cross-sections (barns/atom).

	σ_{L_I}			$\sigma_{L_{II}}$		
	E*	E**	T***	E*	E**	T***
U	644.39 ± 44.06	655.68 ± 26.51	671.29	639.37 ± 15.86	637.68 ± 12.89	638.91
Th	605.98 ± 53.17	704.03 ± 58.78	635.41	536.34 ± 26.37	554.57 ± 13.76	565.84
Bi	493.03 ± 21.90	549.25 ± 38.59	511.43	368.07 ± 14.55	387.37 ± 28.12	360.21
Tl	470.85 ± 33.72	497.38 ± 39.82	477.52	287.09 ± 32.56	309.88 ± 28.03	313.94
Hg	446.94 ± 32.30	446.89 ± 20.04	460.71	285.95 ± 17.14	295.95 ± 15.97	292.74
Hf	366.93 ± 36.36	380.94 ± 45.01	335.73	172.94 ± 18.75	180.63 ± 20.23	160.85

	$\sigma_{L_{III}}$			σ_{L_T}			
	E*	E**	T***	E*	E**	T***	Ref. [11]
U	551.05 ± 23.31	596.84 ± 25.37	622.38	1834.81 ± 171.37	1890.20 ± 113.41	1933	2060 (I. Method)
Th	633.26 ± 24.32	609.17 ± 11.39	619.22	1775.58 ± 191.16	1867.77 ± 166.39	1763	2110 (II. Method)
Bi	470.10 ± 45.83	435.98 ± 36.28	381.57	1331.21 ± 152.01	1372.60 ± 179.65	1253	2090 (III. Method)
Tl	50.04 ± 62.31	320.75 ± 10.42	338.87	1007.98 ± 225.26	1128.01 ± 144.74	1130	1680 (I)
Hg	278.43 ± 36.20	303.74 ± 19.89	318.87	1011.32 ± 162.19	1046.58 ± 100.44	1072	1720 (II)
Hf	181.40 ± 12.81	178.80 ± 10.69	188.58	720.62 ± 118.41	740.37 ± 125.86	685.23	

E* determined experimentally and peaks fitted Gaussians, E** determined experimentally and peaks fitted Gaussians with an exponential tail on their low energy sides, T*** calculated theoretically.

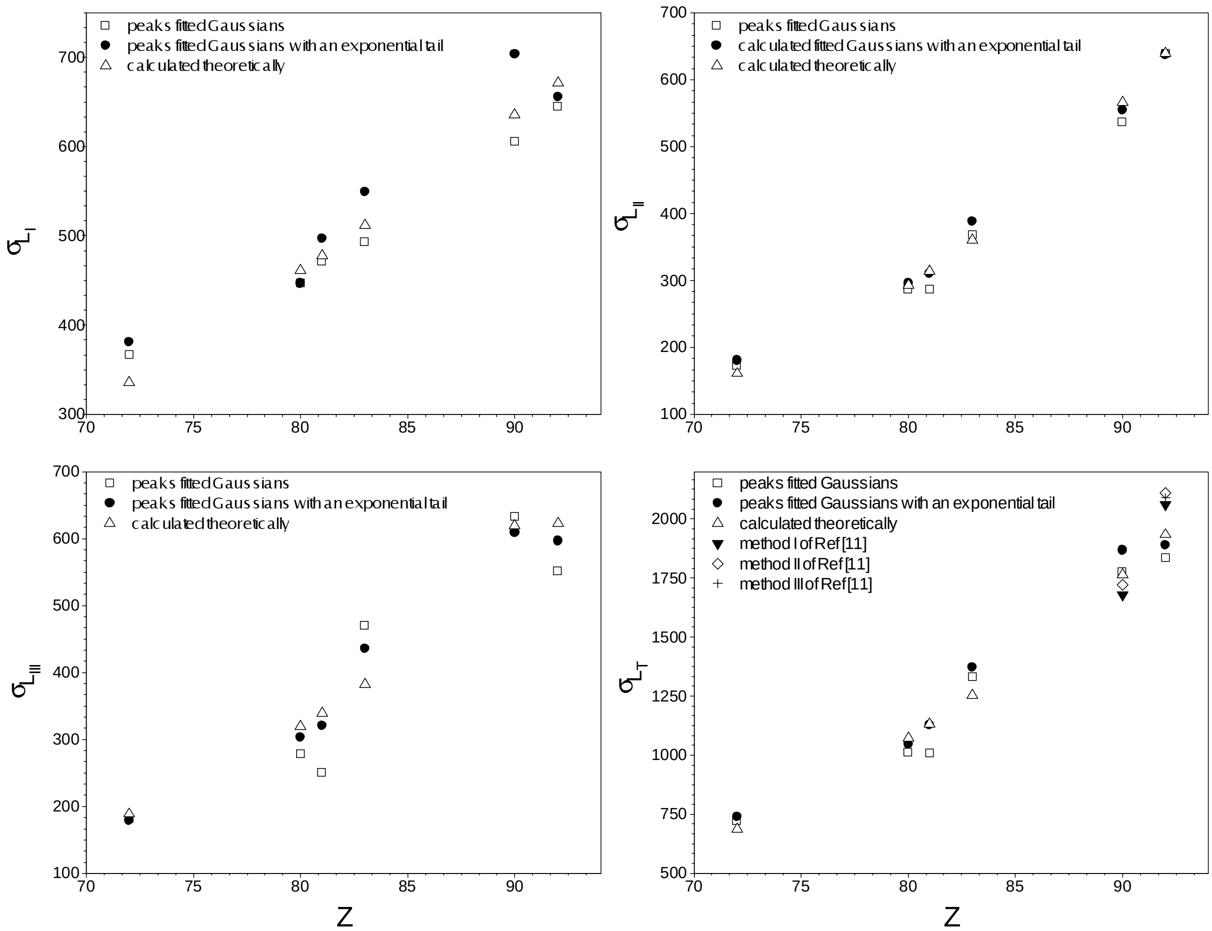

Fig. 4. A comparison of determined photoeffect cross-sections with the theoretical values of Scofield [1] and experimental values exist in the literature [11].

4 Results and discussion

The values of σ_{L_I}, $\sigma_{L_{II}}$, $\sigma_{L_{III}}$, and σ_{L_T} photoeffect cross-sections calculated experimentally and theoretically are tabulated in Table 1. Also included in Table 1 are the σ_{L_T} photoeffect cross-sections of Arora *et al.* [11] determined using three different versions of Sood's method of measuring the absolute yield of fluorescent X-rays when a target is irradiated with a known flux of photons at 59.54 keV.

The L_I subshell photoeffect cross-sections (σ_{L_I}) have been deduced from the measured $L\gamma_1$ and $L\gamma_{2,3,6,8}$ XRF cross-sections by using equation (1). The L_I values agree within experimental errors with theoretical values. The L_{II} subshell photoeffect cross-sections ($\sigma_{L_{II}}$) have been deduced from the measured $L\gamma_1$ and σ_{L_I} XRF cross-sections by using equation (2). The L_{III} subshell photoeffect cross-sections ($\sigma_{L_{III}}$) have been deduced from the determined $\sigma_{L\alpha}$, σ_{L_I}, and $\sigma_{L_{II}}$ XRF cross-sections by using equation (3). Total photoeffect cross-sections (σ_{L_T}) are calculated as the sum of the σ_{L_i} ($i = 1, 2, 3$) photoeffect cross-sections by using equation (4).

The errors in the σ_{L_I}, $\sigma_{L_{II}}$, $\sigma_{L_{III}}$, and σ_{L_T} are 7–10%, 7–12%, 10–12%, and 16–17% when the peaks are represented with a Gaussian; 7–9%, 4–11%, 8–10%, and 13–17% when the peaks are represented with a Gaussian and an exponential tail on their low-energy sides respectively. These errors arise from the maximum experimental errors in the $\sigma_{L\alpha}$, $\sigma_{L\gamma_1}$ and $\sigma_{L\gamma_{2,3,6,8}}$. These errors are typically 8% for $\sigma_{L\alpha}$, and 11% for $\sigma_{L\gamma_1}$ and $\sigma_{L\gamma_{2,3,6,8}}$ when the peaks are represented with the Gaussians. These errors are attributed to the uncertainties in the different parameters using equations (1–3). The errors in the evaluation of the peak areas are about 6%, 10%, 10% for $\sigma_{L\alpha}$, $\sigma_{L\gamma_1}$, and $\sigma_{L\gamma_{2,3,6,8}}$, respectively; the error in $I_0 G\varepsilon$ is less than 5%, the error in the absorption correction β is less than 1%, the error in the thickness measurement is in the order of 1%. When the peaks are represented with the Gaussians and an exponential tail on their low-energy sides, the maximum experimental errors are typically 7% for $\sigma_{L\alpha}$, and 10% for $\sigma_{L\gamma_1}$ and $\sigma_{L\gamma_{2,3,6,8}}$. In this situation, the errors in the evaluation of the peak areas are about 5%, 9%, 9% for $\sigma_{L\alpha}$, $\sigma_{L\gamma_1}$, and $\sigma_{L\gamma_{2,3,6,8}}$, respectively.

L_i ($i = 1, 2, 3$, and Total) photoeffect cross-sections are plotted as a function of the atomic number Z in Figure 4. It is clear from these figures that the measurement of σ_{L_I}, $\sigma_{L_{II}}$, $\sigma_{L_{III}}$, and σ_{L_T} photoeffect cross-sections are in good agreement with the theoretical values. The determined values of the σ_{L_T} photoeffect cross-sections are in good agreement with the theoretical values within experimental errors. But the total L shell photoeffect cross-section values for U are lower than the σ_{L_T} values determined by Arora *et al.* [11]. σ_{L_i}, ($i = 1, 2, 3$) values determined by fitting a Gaussian with an exponential tail on their low energy sides are in very good agreement with the theoretical values (within the experimental errors) compared with values that determined by fitting Gaussians.

References

1. J.H. Scofield, UCRL Report No. 51326, 1973
2. T.K. Umesh, C. Ranganathaiah, Nucl. Instrum. Meth. Phys. Res. B **5**, 472 (1984)
3. A. Karabulut, G. Budak, M. Ertuğrul, Nucl. Instrum. Meth. Phys. Res. B **152**, 202 (1999)
4. G. Budak, A. Karabulut, Ö. Şimşek, M. Ertuğrul, Nucl. Instrum. Meth. Phys. Res. B **129**, 445 (1997)
5. M. Ertuğrul, Ö. Şimşek, O. Doğan, Ü. Turgut, J. Radioanal. Nucl. Chem. Lett. **213**, 37 (1996)
6. T. Changhuan, A. Zhu, L. Taihua, L. Zhengming, Nucl. Instrum. Meth. Phys. Res. B **156**, 1 (1999)
7. F.Q. He, X.F. Peng, X.G. Long, Z.M. Luo, Z. An, Nucl. Instrum. Meth. Phys. Res. B **129**, 59 (1997)
8. L. Sarkadi, T. Mukoyama, Nucl. Instrum. Meth. Phys. Res. B **61**, 167 (1991)
9. S.K. Arora, K.L. Allawadhi, B.S. Sood, Phys. Rev. A **23**, 1147 (1981)
10. H.A. Jahagirdar, B. Hanumiah, S.R. Thontadarya, X-Ray Spectrom. **22**, 163 (1993)
11. S.K. Arora, K.L. Allawadhi, B.S. Sood, J. Phys. B **14**, 1423 (1981)
12. L. Sarkadi, T. Mukoyoma, J. Phys. B **13**, 2255 (1980)
13. J. Semaniak, J. Braziewicz, M. Pajek, T. Cẏzewski, L. Głowacka, M. Jaskoła, M. Haller, R. Karschnick, W. Kretschmer, Z. Halabuka, D. Trautman, Phys. Rev. A **52**, 1125 (1995)
14. J. Semaniak, J. Braziewicz, M. Pajek, A.P. Kobzev, D. Trautmanm, Nucl. Instrum. Meth. Phys. Res. B **75**, 63 (1993)
15. I. Bogdonavić, S. Fazinić, M. Jakšič, Ž. Šmit, Phys. Rev. A **56**, 2860 (1981)
16. H.C. Padhi, B.B. Dhal, V. Nanal, K.G. Prasad, P.N. Tandon, D. Trautman, Phys. Rev. A **54**, 3014 (1996)
17. M. Budnar, Nucl. Instrum. Meth. Phys. Res. B **4**, 303 (1984)
18. R. Hippler, I. McGregor, M. Aydinol, H. Kleinpopen, Phys. Rev. A **23**, 1730 (1981)
19. A. Karabulut, G. Budak, L. Demir, Y. Şahin, Nucl. Instrum. Meth. Phys. Res. B **155**, 369 (1999)
20. G. Budak, A. Karabulut, L. Demir, Y. Şahin, Phys. Rev. A **60**, 2015 (1999)
21. Y. Şahin, A. Karabulut, G. Budak, Appl. Spectr. Rev. **31**, 333 (1996)
22. R.E. van Grieken, A.A. Markowicz, *Handbook of X-Ray Spectrometry: Methods and Techniques* (Marcel Dekker Inc., New York, 1993), pp. 231-232
23. J.L. Campell, J.H. Wang, X-Ray Spectrom. **20**, 191 (1991)
24. D.V. Rao, R. Cesaro, G.E. Giagante, X-Ray Spectrom. **22**, 401 (1993)
25. E.P. Bertin, *Principles and Practise of X-Ray Spectrometric Analysis* (Plenum Press, New York, 1975), p. 117
26. J.H. Hubbell, S.M. Seltzer, NISTIR No. 5632 (1995)
27. J.H. Scofield, 1973, Theoretical photoionization cross-sections from 1 to 1500 keV, UCRL Report No-51326
28. M.O. Krause, J. Phys. Chem. Ref. Data **8**, 307 (1979)
29. J.H. Scofield, At. Data Nucl. Data Tab. **14**, 121 (1974)
30. J.H. Scofield, 1972, UCRL Report No-51231